

AD-A066 702

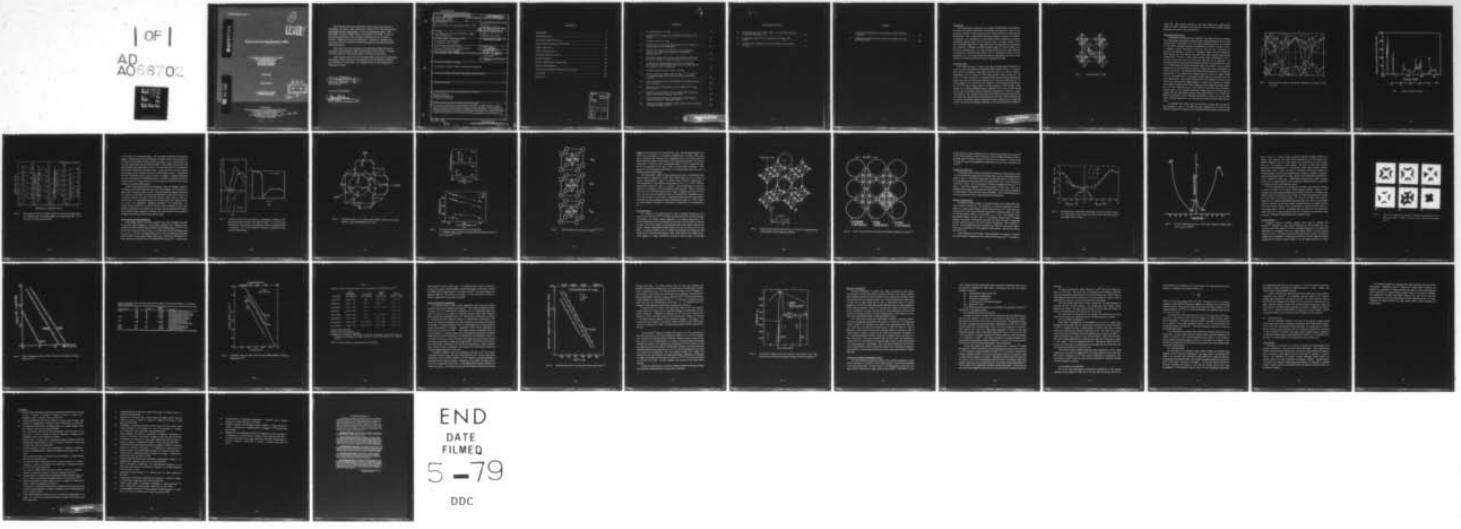
AEROSPACE CORP EL SEGUNDO CA ELECTRONICS RESEARCH LAB  
STATE OF ART OF LAB6 RESEARCH, 1978. (U)

F/G 9/1

UNCLASSIFIED

MAR 79 H KANTER, N M MENDOZA, A B CHASE  
TR-0079(4930-05)-1

F04701-78-C-0079  
NL



12

LEVEL 4

ADA066702

# State of Art of LaB<sub>6</sub> Research, 1978

H. KANTER, N. M. MENDOZA, and A. B. CHASE  
Electronics Research Laboratory  
Laboratory Operations  
The Aerospace Corporation  
El Segundo, Calif. 90245

12 March 1979

Interim Report

APPROVED FOR PUBLIC RELEASE;  
DISTRIBUTION UNLIMITED

DDC  
RECEIVED  
MAY 2 1979  
RESOLVED

DDC FILE COPY

Prepared for  
SPACE AND MISSILE SYSTEMS ORGANIZATION  
AIR FORCE SYSTEMS COMMAND  
Los Angeles Air Force Station  
P.O. Box 92960, Worldway Postal Center  
Los Angeles, Calif. 90009

s/c 392106

79 05 02 035

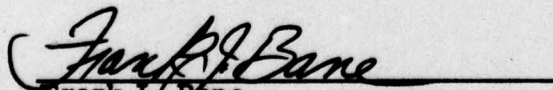
This interim report was submitted by The Aerospace Corporation, El Segundo, CA 90245, under Contract No. F04701-78-C-0079 with the Space and Missile Systems Organization, Contracts Management Office, P. O. Box 92960, Worldway Postal Center, Los Angeles, CA 90009. It was reviewed and approved for The Aerospace Corporation by A. H. Silver, Director, Electronics Research Laboratory. Gerhard E. Aichinger was the project officer for Mission-Oriented Investigation and Experimentation (MOIE) Programs.

This report has been reviewed by the Information Office (OI) and is releasable to the National Technical Information Service (NTIS). At NTIS, it will be available to the general public, including foreign nations.

This technical report has been reviewed and is approved for publication. Publication of this report does not constitute Air Force approval of the report's findings or conclusions. It is published only for the exchange and stimulation of ideas.

  
Gerhard E. Aichinger  
Project Officer

FOR THE COMMANDER

  
Frank J. Bane  
Chief, Contracts Management Office

UNCLASSIFIED

SECURITY CLASSIFICATION OF THIS PAGE (When Data Entered)

REPORT DOCUMENTATION PAGE		READ INSTRUCTIONS BEFORE COMPLETING FORM
1. REPORT NUMBER 18 SAMSO-TR-79-22	2. GOVT ACCESSION NO.	3. RECIPIENT'S CATALOG NUMBER
4. TITLE (and Subtitle) STATE OF ART OF LaB <sub>6</sub> RESEARCH, 1978,		5. TYPE OF REPORT & PERIOD COVERED Interim rept.
7. AUTHOR(s) 19 Helmut/Kanter, Norris M./Mendoza, <del>and</del> Armond B./Chase		6. PERFORMING ORG. REPORT NUMBER 14 TR-0079(4930-05)-1
9. PERFORMING ORGANIZATION NAME AND ADDRESS The Aerospace Corporation El Segundo, Calif. 90245		8. CONTRACT OR GRANT NUMBER(s) 15 F04701-78-C-0079
11. CONTROLLING OFFICE NAME AND ADDRESS Space and Missile Systems Organization Air Force Systems Command Los Angeles, Calif. 90009		10. PROGRAM ELEMENT, PROJECT, TASK AREA & WORK UNIT NUMBERS
14. MONITORING AGENCY NAME & ADDRESS (if different from Controlling Office)		12. REPORT DATE 11 12 Mar 1979
		13. NUMBER OF PAGES 39 (12) 43 p.
		15. SECURITY CLASS. (of this report) Unclassified
		15a. DECLASSIFICATION/DOWNGRADING SCHEDULE
16. DISTRIBUTION STATEMENT (of this Report)  Approved for public release; distribution unlimited		
17. DISTRIBUTION STATEMENT (of the abstract entered in Block 20, if different from Report)		
18. SUPPLEMENTARY NOTES		
19. KEY WORDS (Continue on reverse side if necessary and identify by block number) Electron Emitter Lanthanum Hexaboride Thermionic Emission		
20. ABSTRACT (Continue on reverse side if necessary and identify by block number) An overview of present understanding of physics in LaB <sub>6</sub> is given: Band-structure in bulk and on surface, phonon modes, emission characteristics, surface stability and fabrication methods are touched upon. No attempt at an in-depth correlation of research results has been made, the report is rather a guide to the most recent literature which has appeared on this subject.		

DD FORM 1473 (FACSIMILE)

UNCLASSIFIED

SECURITY CLASSIFICATION OF THIS PAGE (When Data Entered)

79 03 30

392106

## CONTENTS

Introduction . . . . .	7
Crystal Structure . . . . .	7
Electronic Band Structure . . . . .	9
Photon Modes and Superconductivity . . . . .	13
Surface Structure . . . . .	18
Surface Band Structure . . . . .	21
Emission Characteristics . . . . .	21
Surface Oxidation . . . . .	24
Surface Stability and Evaporation . . . . .	29
Surface Contamination . . . . .	33
Fabrication of Metallic Hexaboride Crystals . . . . .	33
Conclusion . . . . .	38
References . . . . .	41

ACCESSION FOR	
DTIC	Write Section <input checked="" type="checkbox"/>
DDC	Dist. Section <input type="checkbox"/>
UNANNOUNCED	<input type="checkbox"/>
JUSTIFICATION	
BY	
DISTRIBUTION/AVAILABILITY CODES	
Dist.	APPLIC. NO. OR SPECIAL
A	

## FIGURES

1.	Crystal Structure of $\text{LaB}_6$ . . . . .	8
2.	Bandstructure of $\text{LaB}_6$ as calculated by Hasegawa and Yanase . . . . .	10
3.	Density of states of $\text{LaB}_6$ . . . . .	11
4.	UPS spectra for the $\text{LaB}_6$ (001) surface as a function of escape angle (in the (010) plane). . . . .	12
5.	Dielectric function and reflectivity as calculated by Suzuki et al. Experimental data are taken from Kierzek-Pecold . . . . .	14
6.	Symmetry points of the simple cubic Brillouin zone and the Fermi surface of $\text{LaB}_6$ as proposed by Arko et al. . . . .	15
7.	a) Raman scattering spectrum for $\text{Eu B}_6$ and $\text{Gd B}_6$ b) Frequency shift of modes with lattice constant varied by various $2+$ as $3+$ metal ions . . . . .	16
8.	Vibration modes of boron lattice in $\text{LaB}_6$ . . . . .	17
9.	Surface structure (upper side) of $\text{LaB}_6$ . P, P' and P'' are dangling bonds which interact with the lanthanum orbitals . . . . .	19
10.	Fig. 9 viewed from top, with position for oxygen arrangement indicated . . . . .	20
11.	Structure of two dimensional energy bands of the $\text{LaB}_6$ (001) surface . . . . .	22
12.	Emission characteristic from a $\langle 100 \rangle$ axial orientation single crystal tip of $\text{LaB}_6$ at $1545^\circ \text{K}^{16}$ . . . . .	23
13.	Field emission patterns as observed in field emission microscope from a $\text{LaB}_6$ tip at $800^\circ \text{C}$ . . . . .	25
14.	Typical Richardson plots for (100), (110) and (111) surfaces of $\text{LaB}_6$ by Oshima et al <sup>18</sup> . . . . .	26

FIGURES (Continued)

15.	Richardson plots for (100), (110), (111) and (346) surfaces of $\text{LaB}_6$ by Swanson et. al . . . . .	28
16.	Evaporation rates for La, LaO and B off $\text{LaB}_6$ (100) surface . . . . .	30
17.	Partial phase diagram of the La-B system in the region of $\text{LaB}_6$ . . . . .	32

TABLES

1.	A list of the thermionic work function and the emission constants . . . . .	27
2.	Summary of work function results and comparison with B/R AES ratios . . . . .	28

### Introduction

This report gives a summary of our present understanding of the physical properties of lanthanum hexaboride. This compound has become of interest for use as cathode material of high emission density with good stability in contaminating environments. Thus, it is presently extensively employed in electron microscopes. Its potential as an alternative to conventional cathode materials has spawned considerable research effort over the last few years. Aerospace interest results from the possible application of  $\text{LaB}_6$  cathodes for beam generation in space borne TWT amplifiers. Although for emission purposes  $\text{LaB}_6$  is of prime interest other hexaboron compounds have very similar physical properties and in many instances are discussed in conjunction with  $\text{LaB}_6$  in order to elucidate the effect of atomic parameters, etc. It is believed that the literature index given at the end is fairly complete for physics related work which has appeared since 1968.

### Crystal Structure

The crystal structure of  $\text{LaB}_6$  (or any  $\text{MB}_6$  compound where M stands for a metal ion of the earth alkaline or rare earth series) is shown in Fig. 1. It forms a cubic lattice of octahedral boron cages with the metal ion in the bcc position. Depending on size or valency of M the lattice constant varies between 4.17 and 4.29 Å. The boron framework is covalently bonded sharing nearly 20 electrons per cage, where about 2 electrons are supplied by the metal ion whose bond to the crystal appears to be of primarily ionic character. The remaining electron(s) (one per M for the case of  $\text{LaB}_6$ ) impart a metallic character to the material.  $\text{LaB}_6$  behaves as a metallic conductor having a resistivity of  $8.9 \mu\Omega \text{ cm}$  at  $20^\circ\text{C}$  ( $58 \mu\Omega \text{ cm}$  for La) with a positive thermal coefficient of resistance of  $0.060 \mu\Omega \text{ cm deg.}^{-1}$ . The stability of the compound is determined by the boron framework rather than by the metal atom, and as long as the electronic requirements of this framework are maintained, the stability appears unaffected by other changes, as for instance the creation of vacant sites through La diffusion, or even the incorporation of different

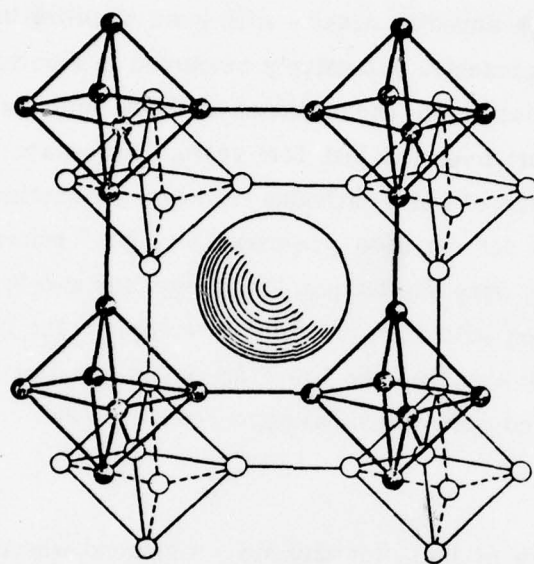


Fig. 1. Crystal Structure of  $\text{LaB}_6$

metal ions. The stability accounts for the high melting point (approximately 2200°C to 2700°C, depending on stoichiometric ratio) and the chemical inertness, properties more akin to those of pure boron.

### Electronic Band Structure

Band structure calculations have advanced to the stage where fair correlation with experimental observations exists although detailed agreement has not been attained as yet. The results of the most recent calculation of the  $E$  vs.  $k$  relation for the various crystalline directions by Hasegawa and Yanase<sup>2</sup> is shown in Fig. 2. In contrast to earlier calculations, which took only the B 2s, p electrons into account<sup>3</sup> and appeared to arrive at a reasonable density of states distribution which agreed with data deduced from XPS (X-ray photo electron spectroscopy) measurements<sup>4</sup>, the more recent results indicate strong hybridization of the La 5d and 6s bands with those of B which can definitely not be neglected. The calculations shown in Fig. 2 are self-consistent and have been carried out by means of a nonrelativistic symmetrized augmented plane wave method. The La d bands appear near the Fermi energy,  $E_F$ , and show strong wave vector dependence;  $E_F$  cuts one such band. The density of states distribution deduced from this data are shown in Fig. 3. The valence states between 3 and 11 eV below  $E_F$  consist mainly of the B 2 s.p states and it is this group of states which has been observed in the XPS measurements. More recent measurements<sup>5</sup> on the density of states by UPS (Ultra-Violet Photoelectron Spectroscopy), a method more suitable for reliable spectroscopy of states near the Fermi energy, and whose results are shown in Fig. 4, have not been interpreted as yet with respect to the above band calculations. Since the peak at 2 eV has been identified as being caused by a surface state, it appears that the experimental spectrum does indeed indicate a 3.5 eV wide "gap" below  $E_F$  as apparent in Fig. 3. Definite conclusions, of course, can only be drawn after a detailed evaluation of the convolution of initial and final states has been made.

A comparison with optical reflection data<sup>6</sup> does not agree very well with the band structure of Fig. 2. This data has been interpreted on the basis of the dielectric properties of metals, with the dielectric function being a strong function

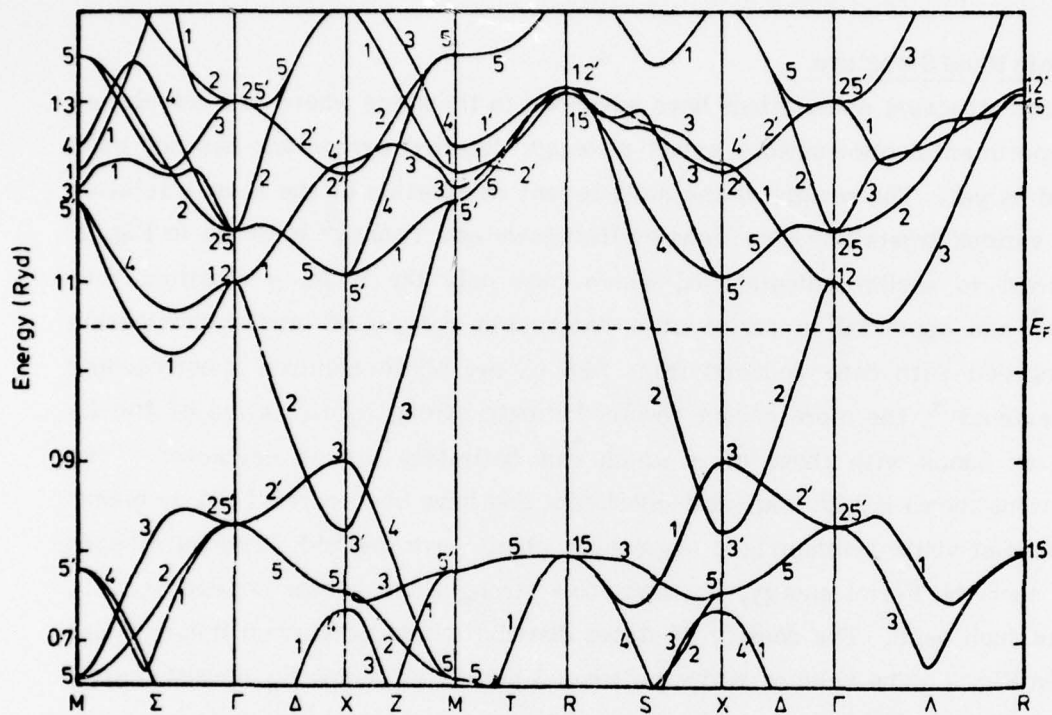


Fig. 2 Bandstructure of LaB<sub>6</sub> as calculated by Hasegawa and Yanase.<sup>2</sup> (1 Ryd ≡ 13.6 eV)

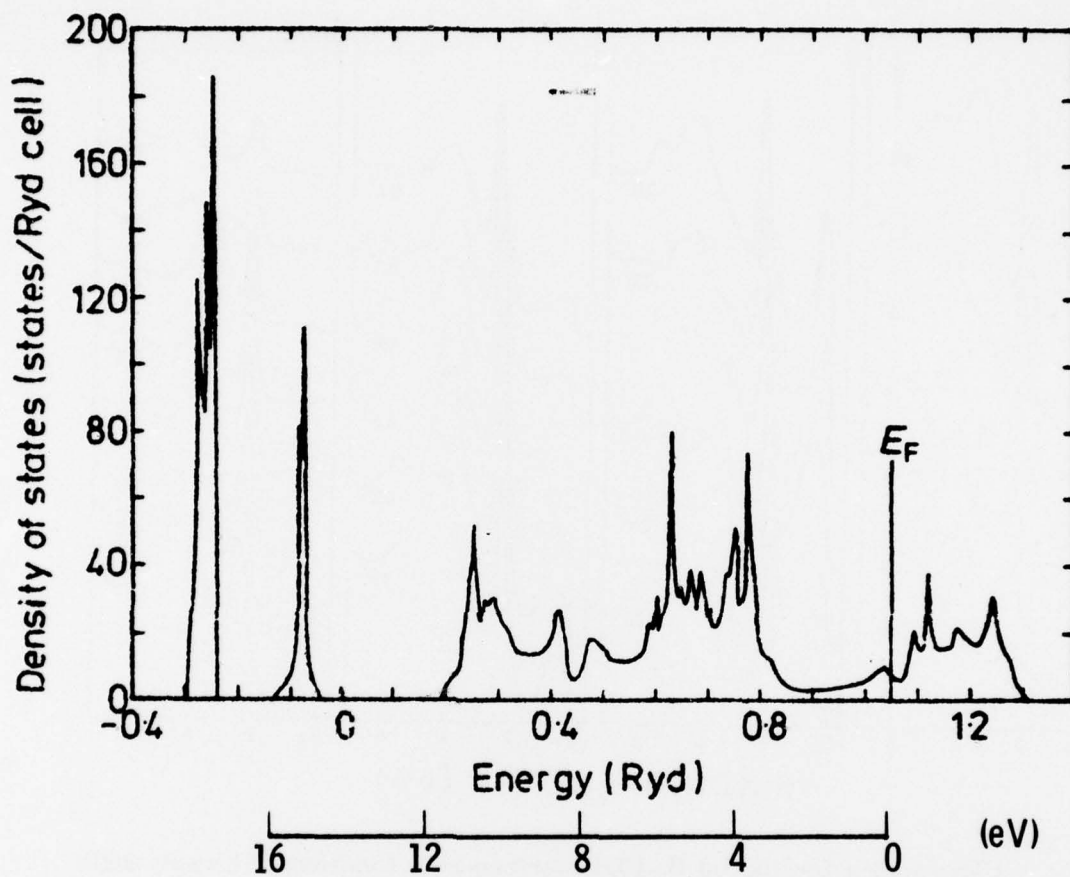


Fig. 3. Density of states of  $\text{LaB}_6^{.2}$

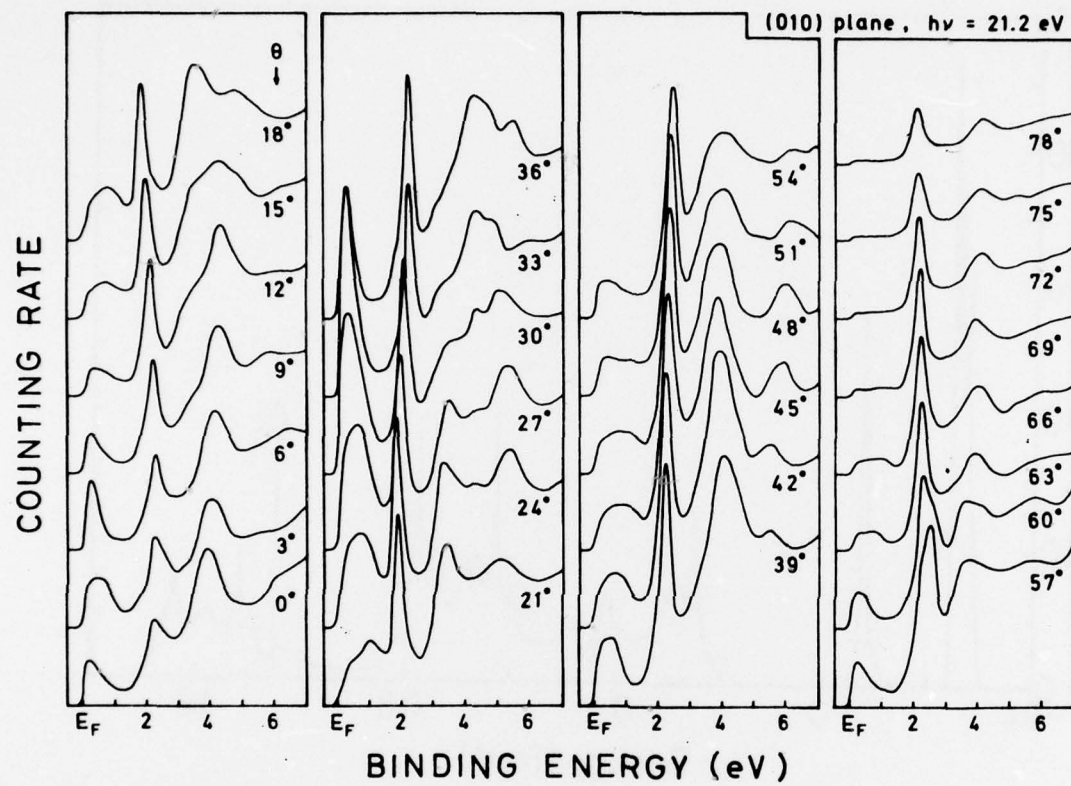


Fig. 4. UPS spectra for the La B<sub>6</sub> (001) surface as a function of escape angle (in the (010) plane). The incident angle of the exciting light ( $h\nu = 21.2$  eV) is 20° from the surface normal.<sup>5</sup>

of the density of states distribution. For intra band transitions Drude analysis applies. Taking free electron and interband contributions into account, Suzuki, et al.,<sup>6</sup> arrive at a calculated dielectric function as shown in Fig. 5 which agrees very well with experimental data by Kierzek-Pecold.<sup>7</sup> They deduce from this data that the top of the main valence band is about 1 eV below the bottom of the conduction band, which contrasts with the data of Fig. 2, where the top of the main valence band reaches or even exceeds the bottom of the conduction band. Consequently, the band calculations tend to give too small a bandgap, a tendency apparently common to standard band calculation methods. However, as deduced from Fermi surface studies, the free electrons are not of s-character, where the free electron model can be unambiguously applied.

Fermi surface determinations by deHaas-van Alven and magneto resistance techniques, made independently by Arko et al.<sup>8</sup> and Ishizawa et al.<sup>9</sup> arrived at a shape which consists, as shown in Fig. 6, of nearly spherical ellipsoids located at the X points of the Brillouin Zone and interconnected by narrow necks. (Note that this shape contrasts with that of the free electron model where the sphere is centered (at  $\Gamma$ ) in the Brillouin Zone.) Here the neck shape is not entirely certain as yet due to the possibility of "Magnetic breakdown" in the experiments. The cyclotron mass is about  $0.7 m_0$  and the carrier density obtained from the Fermi surface corresponds to one electron per unit cell. The band calculations<sup>2</sup> indicate a Fermi surface whose character is consistent with that obtained by measurement, although the calculated neck sizes are much too large.

#### Phonon Modes and Superconductivity

Some phonon modes in the boron structure have been investigated through Raman-active light scattering on various  $MB_6$  compounds, from which the force constants and their variation with ion radius could be deduced (Fig. 7).<sup>10,11,12</sup> The Raman-active modes are shown in Fig. 8. It is found that the B-B stretching modes ( $A_{1g}$  and  $E_g$  of Fig. 8) are strongly affected by the inter-octrahedral bond length) while the B-B-B valence angle bending mode ( $F_{2g}$ ) is affected by screening of the metal electrons as deduced from the dependence on valency of M. It furthermore

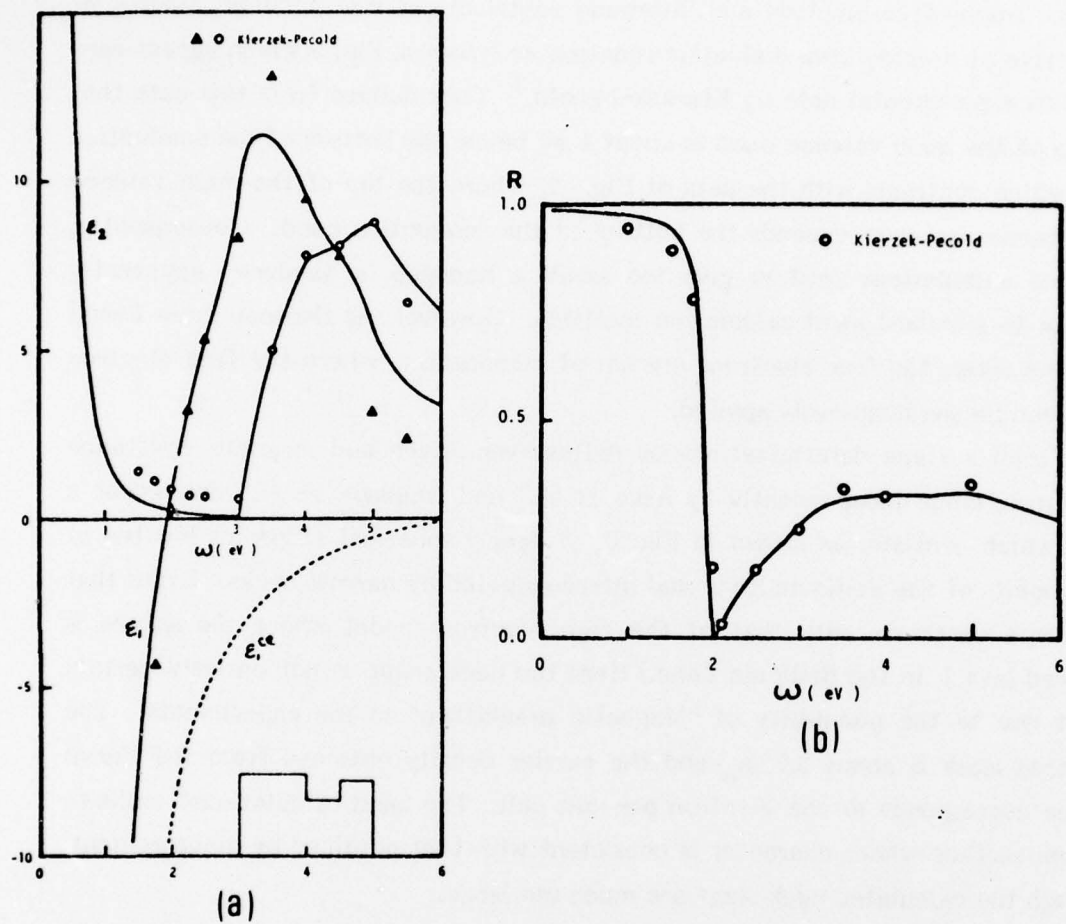


Fig. 5. Dielectric function and reflectivity as calculated by Suzuki et al.<sup>6</sup> Experimental data are taken from Kierzek-Pecold.<sup>7</sup> In the lower right hand position of (a) the peak of the density of states in the valence band is indicated.  $\epsilon_1^{ce}$  is the dielectric function as deduced for free electrons (Drude model).

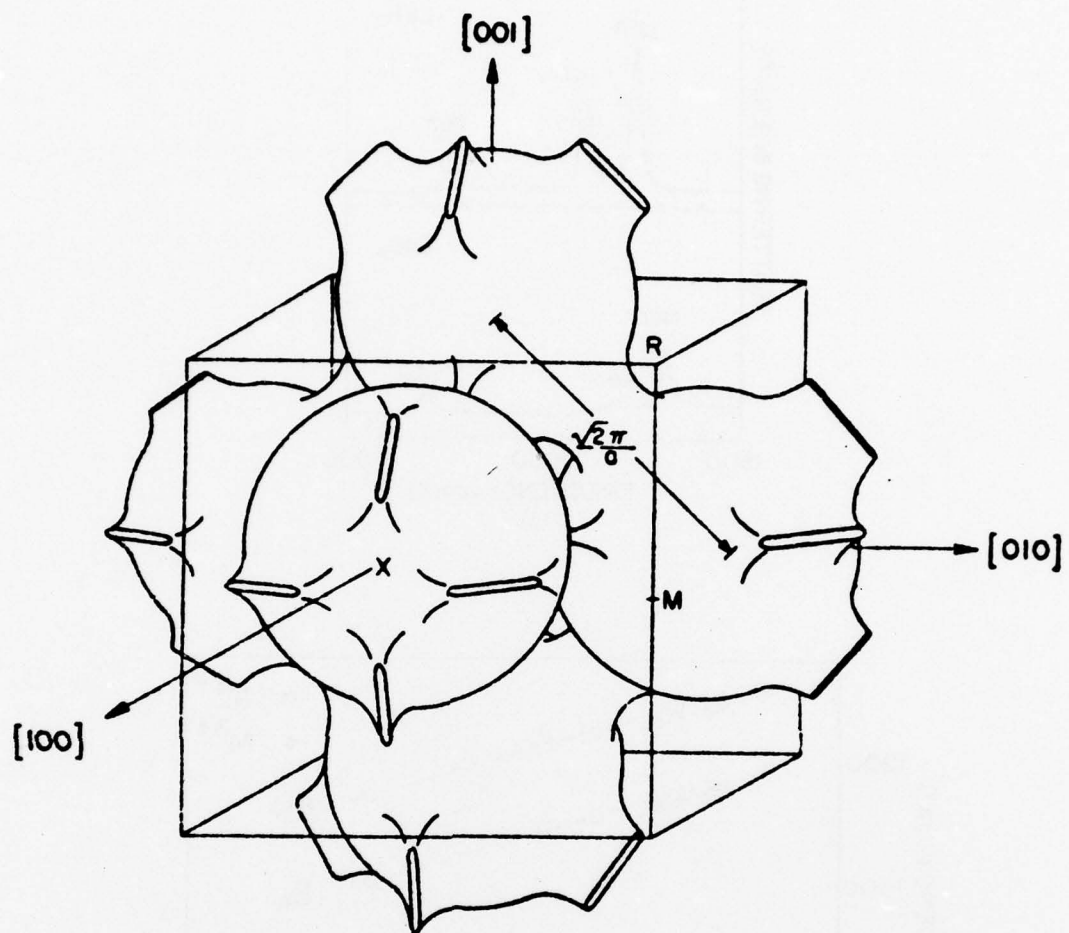


Fig. 6. Symmetry points of the simple cubic Brillouin zone and the Fermi surface of  $\text{LaB}_6$  as proposed by Arko et al.<sup>8</sup>

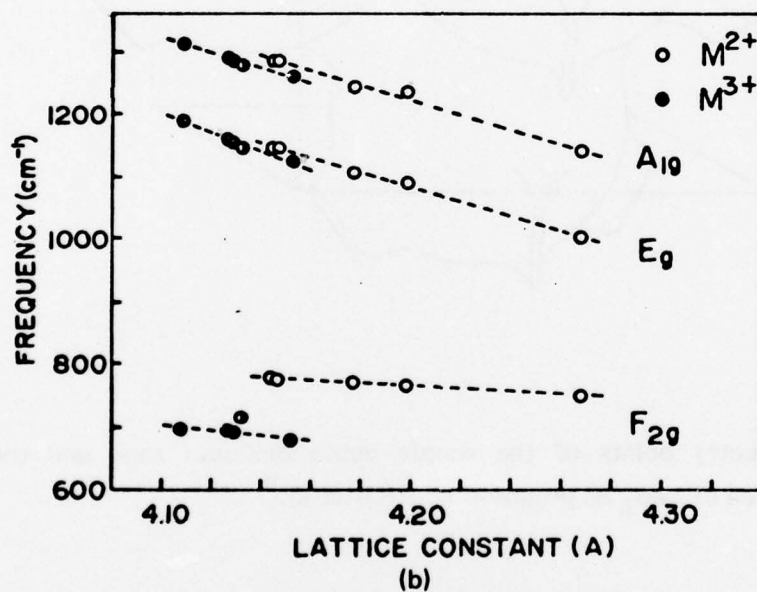
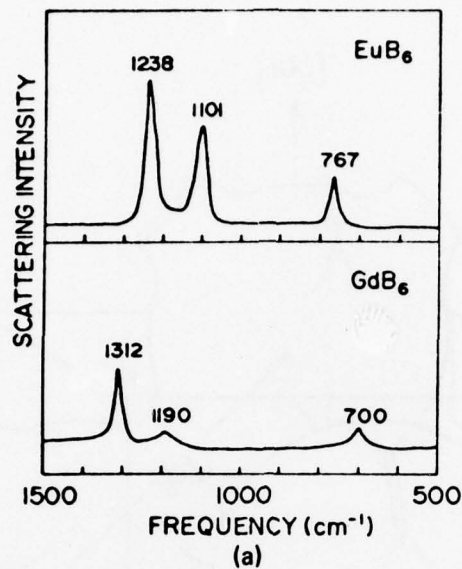


Fig. 7. a) Raman scattering spectrum for  $\text{EuB}_6$  and  $\text{GdB}_6$   
 b) Frequency shift of modes with lattice constant varied by various 2+ as 3+ metal ions.  
 10, 11, 12

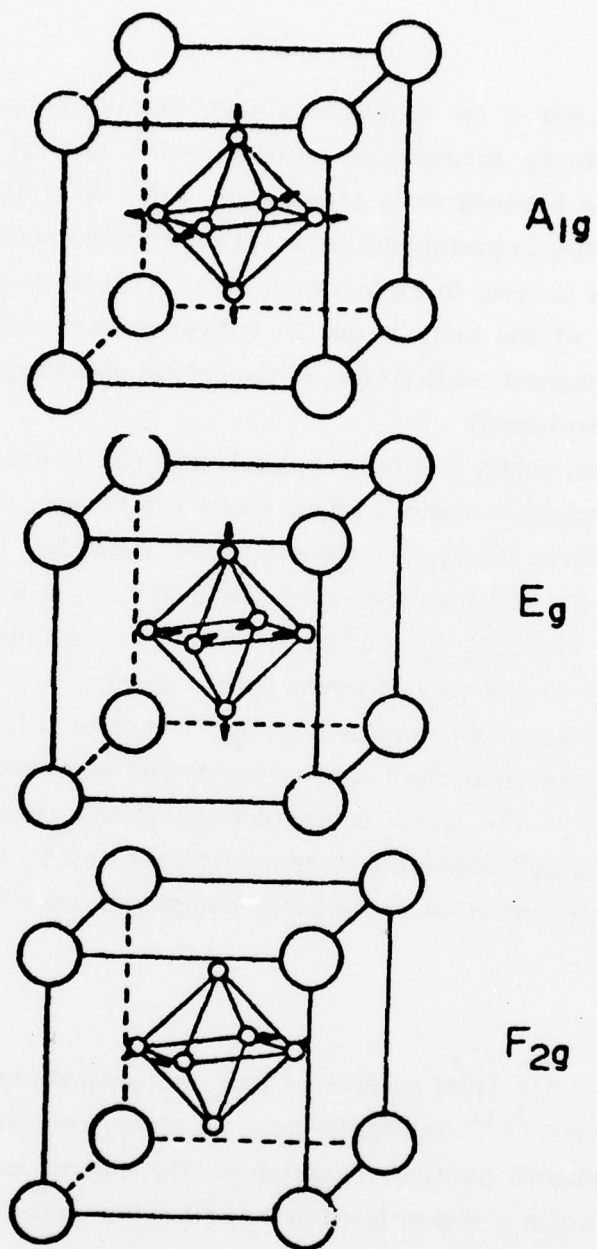


Fig. 8. Vibration modes of boron lattice in  $LaB_6$ .<sup>10, 11, 12</sup>

suggests an ionic character of the metal-boron bond. This conclusion appears to be confirmed by resistivity vs. temperature measurements<sup>1</sup> on single crystal  $\text{LaB}_6$  with a resistivity ratio between room temperature and 4 K of 450:1, where the authors found it necessary to postulate a polar optical phonon branch with a Debye temperature  $\theta = 920$  K in order to explain their data. At room temperature about 30% of the resistivity of the  $\text{LaB}_6$  is due to optical phonon scattering. There appears to be no independent confirmation of the optical phonon spectrum (by, for instance, infrared spectroscopy).

The strong phonon modes of  $\text{MB}_6$  compounds give rise to exceptionally large electron-phonon enhancement factors which would expect one, on the basis of common superconductive theory, to observe large transition temperatures.<sup>13</sup> (Naive application of the McMillan theory results in  $27 < T_c < 61^\circ\text{K}$ ). Inductive measurements reveal for  $\text{LaB}_6$   $T_c = 0.122^\circ\text{K}$ . This striking failure of theory is believed to be related to the very different phonon spectra - "hard" boron-based modes and "soft" lanthanum-based modes in  $\text{LaB}_6$  - compared with those of Nb or other more common superconductors used in the derivation of McMillan's theory. Note that  $\text{YB}_6$  has a  $T_c \approx 7^\circ\text{K}$ , but Y is superconducting only under high pressure. In contrast La metal is superconducting at temperatures below  $T_c = 4.9^\circ\text{K}$ . Clearly the superconductive properties of metal-boron compounds are not understood as yet.

#### Surface Structure

The structure of the (100) surface of  $\text{LaB}_6$  is presently believed to be as shown in Fig. 9 and Fig. 10<sup>5,14</sup>. The rather large La atoms form the terminal plane and because of its electro positive character vs. the electro negative one of B forms a dipole layer which is responsible for the rather low work function observed on  $\text{LaB}_6$ . LEED data indicate no reconstruction (from cubic bulk) to occur at the surface. Several experimental results indicate that the La atoms form the top layer: a) Surface oxidation does not change the structure but reduces the AES (Auger Electron Spectroscopy) signal of boron, while leaving the La signal intact, which suggests an oxygen arrangement as shown in Fig. 10 where the terminal

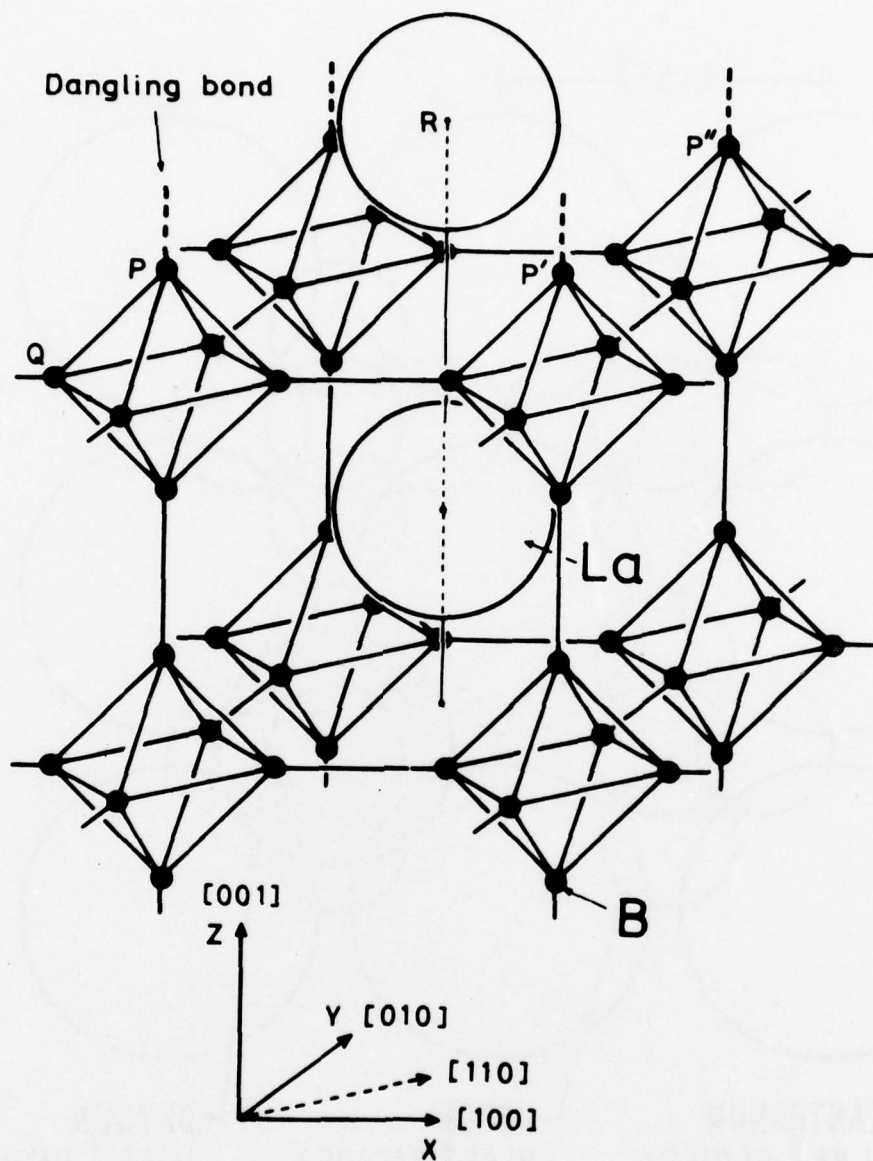


Fig. 9. Surface structure (upper side) of  $\text{LaB}_6$ . P, P' and P'' are dangling bonds which interact with the lanthanum orbitals.<sup>5</sup>

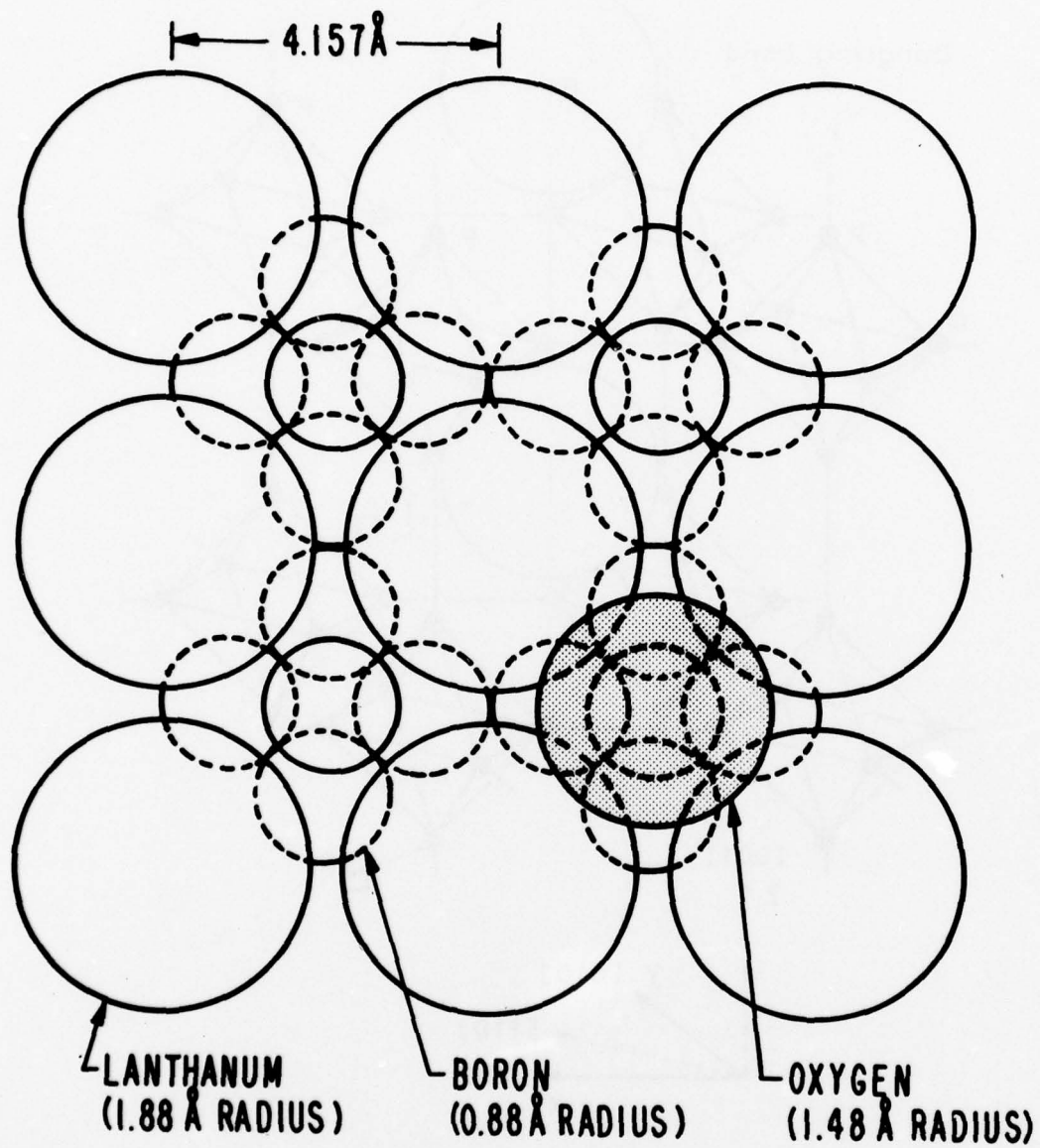


Fig. 10. Fig. 9 viewed from top, with position for oxygen arrangement indicated.<sup>14</sup>

plane consists of oxygen sitting on top of B in the grooves between the La atoms.<sup>14</sup>  
b) The other indication arrives from angular resolved energy loss spectra, which at glancing angle of electron escape (from only the top two layers or so) show strong La lines, but weak B lines suggesting "shadowing" by the top layer consisting of La atoms.<sup>15</sup>

#### Surface Band Structure

From angle resolved electron loss spectra<sup>5</sup> obtained by UPS and shown in Fig. 4, a two-dimensional energy band of the (100) surface has been determined which is shown in Fig. 11. The authors argue that the upper band cannot be derived from boron dangling bonds alone since then the energy widths in the  $\Gamma X$  and  $\Gamma M$  direction could not be similar. The bond coupling  $P P'$  would be stronger than that of  $P P''$  in Fig. 9. The solution suggested is the shown position of the La ion. Now the B dangling bond overlaps with the electron-orbital of the La atom and an equalization of bond strength in both directions appears plausible. A more detailed analysis of the surface bonds will have to await bandstructure calculations.

#### Emission Characteristics

Thermionic emission density is a strong function of the crystal plane from which emission is observed. The anisotropy of thermionic electronic emission values for a single crystal emitter cathode is shown in Fig. 12.<sup>16</sup> These data were obtained from a  $\langle 100 \rangle$  axial orientation crystal with a naturally faceted tip, which was electrolytically etched to a tip radius of 1 - 2  $\mu m$ . The electrons were accelerated towards an anode with a 1 mm aperture, behind which a Faraday collector was placed. Noteworthy is the fact that nearly an order of magnitude stronger emission occurs in the  $\langle 110 \rangle$  direction compared to  $\langle 100 \rangle$  direction of the tip. The corresponding current densities were  $50 A/cm^2$  and  $5 A/cm^2$  respectively, and are believed not to be assisted by field emission. (The tip field was of order  $10^6$  V/cm.)

A good indication of the crystal surface dependence of emission is obtained from field emission measurement from  $\langle 100 \rangle$  oriented  $LaB_6$  tips.<sup>17</sup> An example is

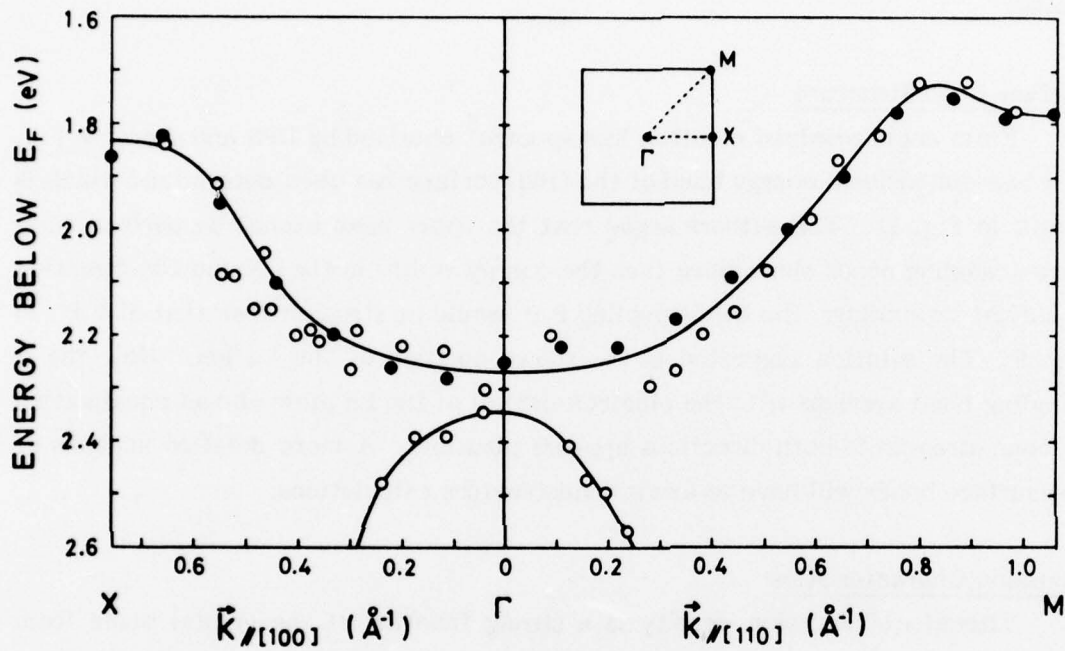


Fig. 11. Structure of two dimensional energy bands of the La B<sub>6</sub> (001) surface. The experimental points, shown by open circles, have been reduced from higher Brillouin zones.<sup>5</sup>

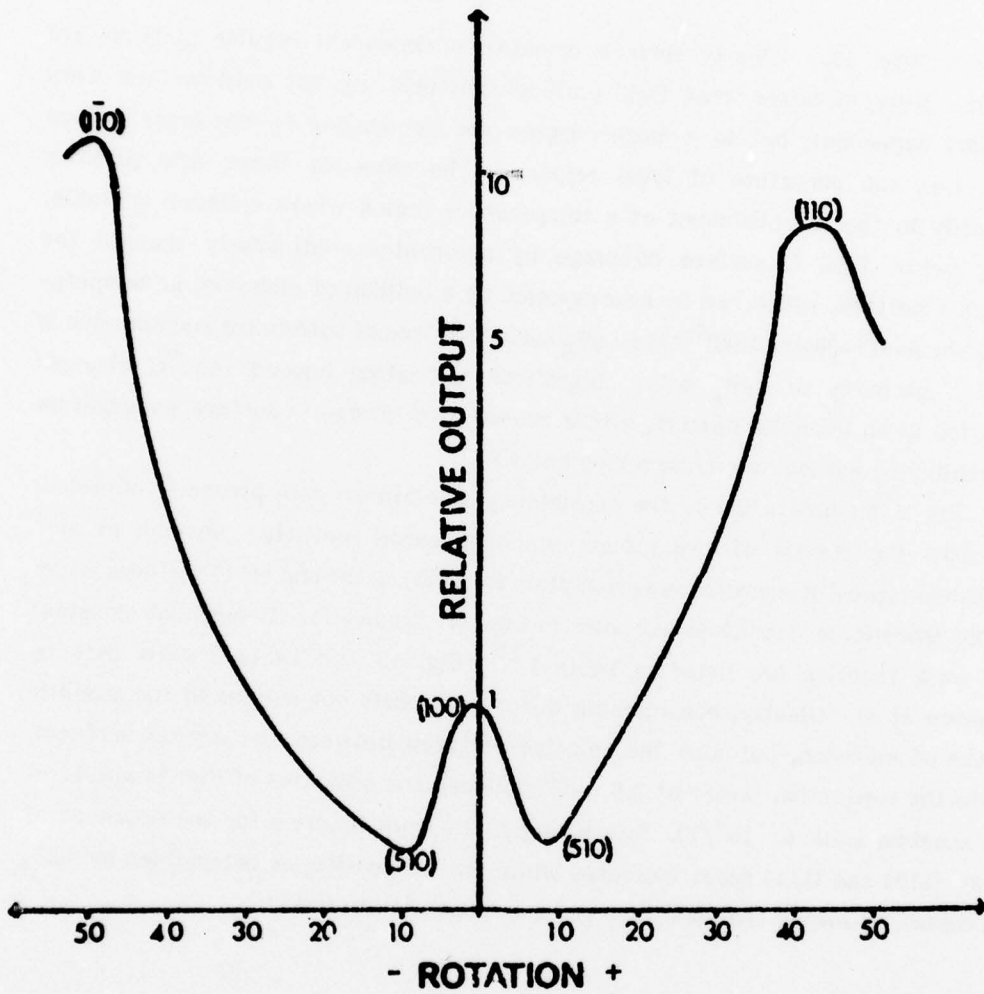


Fig. 12. Emission characteristic from a  $\langle 100 \rangle$  axial orientation single crystal tip of  $\text{LaB}_6$  at  $1545^\circ\text{K}$ .<sup>16</sup>

shown in Fig. 13. Clearly surface orientation dependent regular patterns are visible. Note, however, that field emission patterns are not only surface work function dependent, but to a larger degree are determined by the local surface field, i.e., the curvature of local regions. The value of these data pertains primarily to the establishment of a temperature region where emission is stable. While below 1300 C surface coverage by adsorbates continuously changes the emission pattern, which can be accompanied by a buildup of emission, at temperatures between 1400 and 1600°C the LaB<sub>6</sub> surface is free of adsorbates and emission is truly a property of LaB<sub>6</sub> only. Significantly heating beyond 1600°C changes emission to an irregular pattern, either caused by a change in surface composition or possibly by carbon outdiffusion (see below).

For a demonstration of the consistency of emission data presently obtained, we show the results of two groups which appeared recently. Oshima et al.<sup>18</sup> published typical Richardson emission plots for (100), (110) and (111) surfaces under stable thermionic conditions as shown in Fig. 14. Values for Richardson's constant and work function are listed in Table 1.<sup>18</sup> Fig. 15 and Table 2 show data by Swanson et al. Clearly, considerable difference exists not only as to the absolute values of emission, but also the relative emission between the crystal surfaces. (Note the conversion factor of  $2.8 \cdot 10^6$  between the ordinates of Fig. 14 and 15 at the abscissa value  $6 \cdot 10^4/T$ ). Interestingly, the work function for the sequence of (100), (110) and (111) faces increases while the La density, as determined by AES, decreases. However the (346) face gives an exception to this.

#### Surface Oxidation

Extensive studies on surface oxidation were made by Goldstein and Szostak.<sup>14</sup> Oxidation of LaB<sub>6</sub> surfaces increases the work function and consequently lowers the emission. At room temperature exposure to O<sub>2</sub> leads to the formation of a monolayer, which on a (100) surface results in a work function change of 1.4 eV. No further increase occurs with further exposure. Initially the oxygen layer is amorphous. Heating beyond 1000°K (in vacuum) leads to a surface arrangement of oxygen as shown in Fig. 10, i.e., the oxygen atoms form a surface

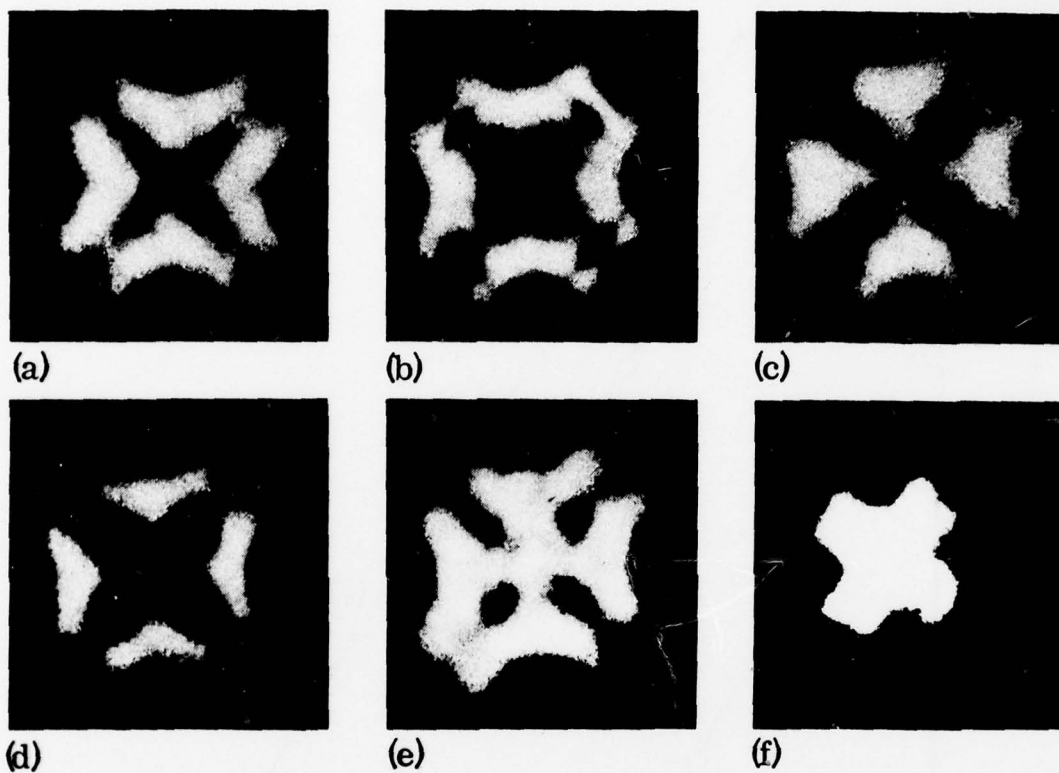


Fig. 13. Field emission patterns as observed in field emission microscope from a  $\text{LaB}_6$  tip at  $800^\circ\text{C}$ . Change in pattern is due to variation of adsorbate layers.<sup>17</sup>

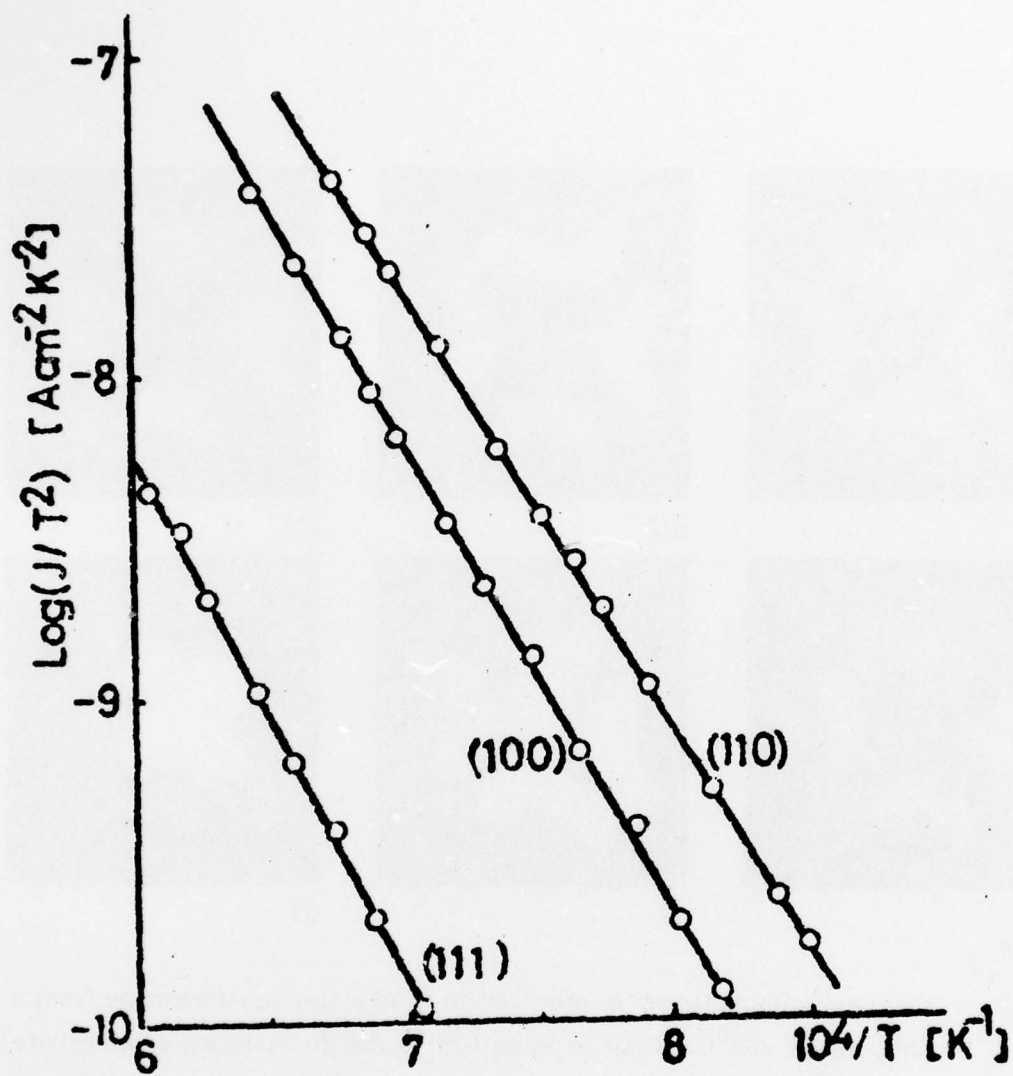


Fig. 14. Typical Richardson plots for (100), (110) and (111) surfaces of  $\text{LaB}_6$  by Oshima et al.<sup>18</sup>

TABLE I. A list of the thermionic work function and the emission constants. The work function for specimen 6 is measured by CPD at  $5 \times 10^{-10}$  Torr.<sup>18</sup>

Specimens (face)	$\phi$ (eV)	$A$ (A/cm <sup>2</sup> K <sup>2</sup> )	Pressure (Torr)	Comments
1 (100)	2.86	82	$4 \times 10^{-8}$	After heating at 1200°C for 20 h
	2.88	85	$4 \times 10^{-8}$	After further heating at 1200°C for 10 h
	2.85	72	$3 \times 10^{-8}$	After further heating at 1200°C for 10 h
	2.89	86	$2.5 \times 10^{-8}$	After further heating at 1400°C for 5 h
2 (100)	2.87	48	$1.5 \times 10^{-8}$	After heating at 1200°C for 20 h
	2.88	84	$7 \times 10^{-9}$	After air-exposing for 1 h followed by heating at 1400°C for 1 h
3 (110)	2.66	14	$1.5 \times 10^{-8}$	After heating at 1200°C for 25 h
	2.65	47	$8 \times 10^{-8}$	After repolishing followed by heating at 1400°C for 1 h
4 (110)	2.68	57	$2 \times 10^{-8}$	After heating at 1300°C for 15 h
5 (111)	3.4	71	$7 \times 10^{-8}$	After heating at 1300°C for 15 h
6 (111)	3.6	...	$5 \times 10^{-10}$	Measured by CPD method

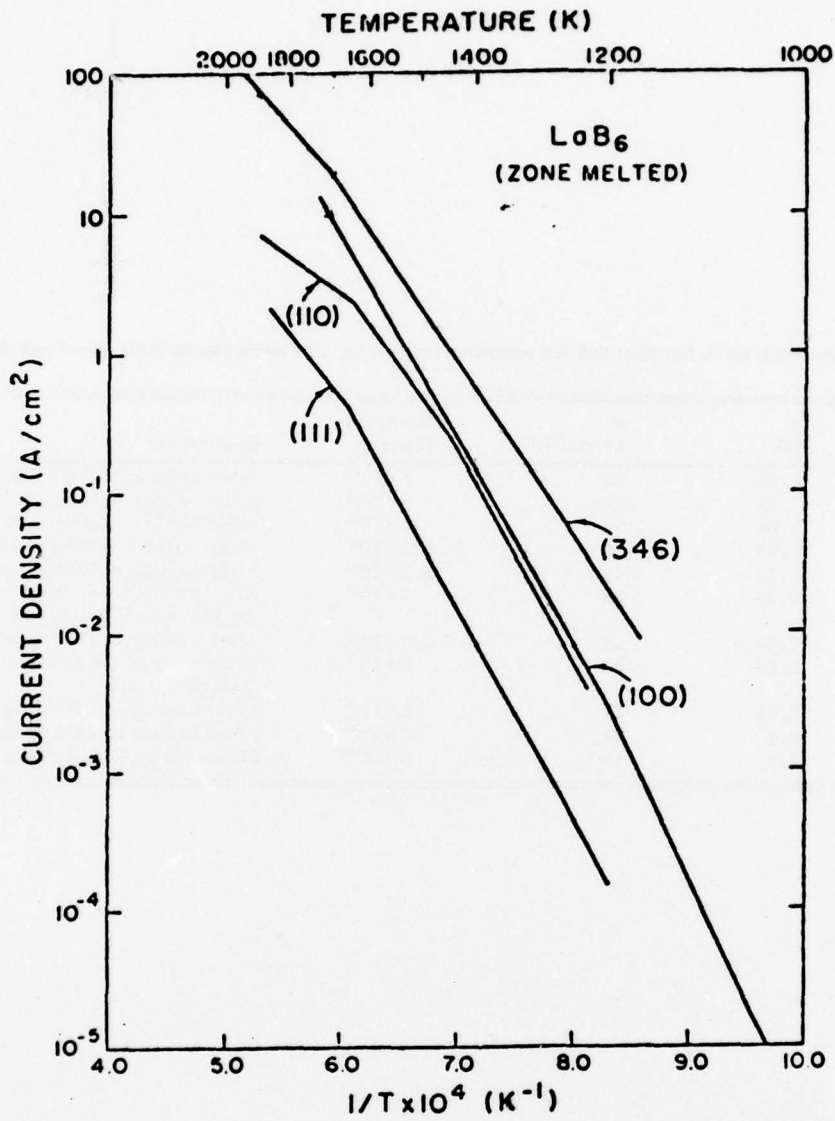


Fig. 15. Richardson plots for (100), (110), (111) and (346) surfaces of LaB<sub>6</sub> by Swanson et. al.<sup>19</sup>

Table 2.

Summary of work function results and comparison with B/R AES ratios.<sup>19</sup>

Material	$\phi_e$ (eV) Thermionic (at 1600 K)	J (A/cm <sup>2</sup> )*** (at 1600 K)	$\phi_f$ (eV) FERP (at 300 K)	B/R**** (AES at 5 kV)
LaB <sub>6</sub> (110)*	2.60 ± .05	1.95	2.8 ± .05	3.4 ± .1
LaB <sub>6</sub> (111)*	2.90 ± .05	0.22	2.8 ± .1	5.0 ± .2
LaB <sub>6</sub> (100)*	2.52 ± .05	3.5	2.6 ± .05	3.4 ± .1
LaB <sub>6</sub> (346)	2.41 ± .05	7.8		4.1 ± .2
LaB <sub>6</sub> (100)**	2.70 ± .05	1.0	2.3 - 2.6	3.3 ± .1
CeB <sub>6</sub> (100)**	2.62 ± .05	1.7	2.5 ± .05	2.2 ± .1
SmB <sub>6</sub> (100)**	3.92 ± .05	1.4 × 10 <sup>-4</sup>	4.3 ± .05	4.0 ± .3
BaB <sub>6</sub> (100)**	3.40 ± .05	5.9 × 10 <sup>-3</sup>	3.4 ± .05	6.8 ± .4

\*Zone melted material

\*\*Molten Al flux growth

\*\*\*Zero field current densities

\*\*\*\*Based on elemental sensitivity of B(179) and R(MNN) transitions and including corrections for atomic densities between elemental and compound forms.

FERP = Field emission retarding potential method.

mesh identical to that of clean  $\text{LaB}_6$ . At temperatures above  $500^\circ\text{C}$  the reaction of  $\text{LaB}_6$  with oxygen increases sharply. Strong indications of oxide state B and La are clearly seen by chemical shifts in the Auger spectra.<sup>20</sup> The color changes from purple to deep red. The surface is amorphous. A total work function change of 2.42 eV compared with clean  $\text{LaB}_6$  is observed.

#### Surface Stability and Evaporation

An extensive study of (001) surface evaporation under clean and oxidized conditions was done by Goldstern and Szostak.<sup>14</sup> They measured evaporation rates as shown in Fig. 16. Note that the evaporation of La is considerably larger than that of B (ratio 5:1) in contrast to previously reported results which indicated nearly stoichiometric evaporation rates.<sup>21</sup> However, no La enrichment is observed (as measured with AES) leading the authors to conclude that no activation of the surface for emission is necessary, but, that the surface is the natural one obtained by cleavage. A further conclusion is that the replenishment of La at the surface is readily accomplished by diffusion. Evaporation rates become appreciable at temperatures in excess of  $1500^\circ\text{C}$ . With oxygen present, evaporation occurs at lower temperature. Oxides, however, can be eliminated by heating into the  $1600^\circ\text{C}$  range with only La and B remaining. The correlation of the evaporation rates of B, La and other rare earth metals with their metal vapor pressures has these authors postulate a surface layer at large temperature ( $1400^\circ\text{C}$  and above) which is akin to the metal phase per constituent, more so than the  $\text{LaB}_6$  phase, to which the surface layer reverts at lower temperatures. The blurring of the LEED pattern under this condition appears supportive of this view.

Somewhat different results were obtained by Swanson et al.<sup>19</sup> who studied vaporization rates of  $\text{LaB}_6$  and other metal borides (Ca, Ba, Ce) and found great variability in the activation energies,  $E$ , for the evaporation process depending on stoichiometry and impurity content. Usually  $E_B \leq E_M$ , which correlates with a B/M ratio considerably smaller than 6. Long heating times tended to increase and equalize  $E_B$  and  $E_M$ . The largest  $E_B$ ,  $E_M$  and thus the lowest vaporization rate was

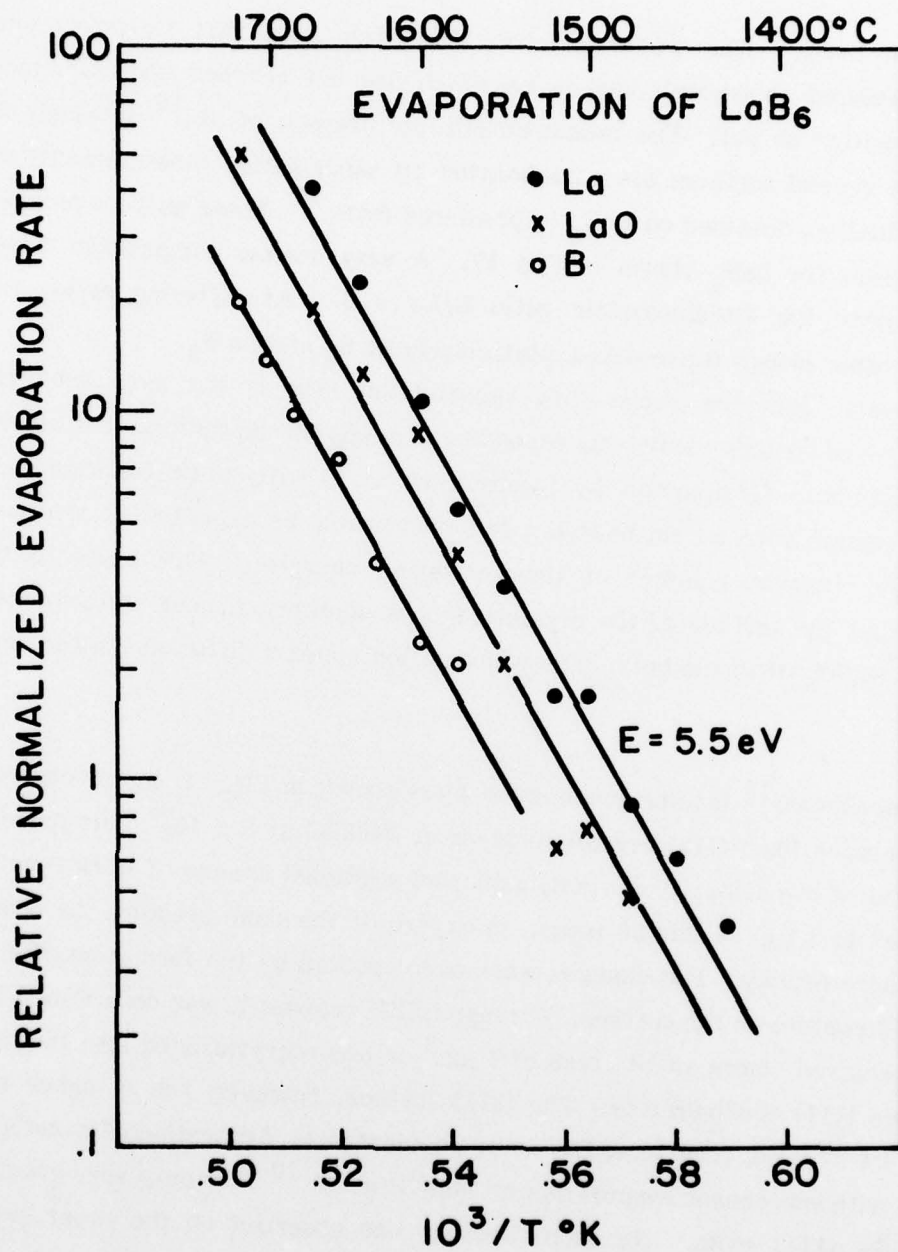


Fig. 16. Evaporation rates for La, LaO and B off LaB<sub>6</sub> (100) surface.<sup>14</sup>

obtained with  $\text{LaB}_6$ . One would conclude from this data that Goldstein and Szostak<sup>14</sup> measured on crystals rich in La which had not reached near stoichiometric composition as yet. The measurements by Swanson et al.,<sup>19</sup> obtained on various single crystal surfaces are corroborated by vaporization measurements of Storms and Mueller, obtained on  $\text{LaB}_6$  in powdered form.<sup>22</sup> These authors propose a phase diagram for  $\text{LaB}_6$  shown in Fig. 17. A very narrow composition range exists only near the stoichiometric ratio  $\text{B/La} = 6$ . At differing ratios the existence of other phases is presumed, particularly  $\text{LaB}_4$  and  $\text{LaB}_9$ .

It appears from the above that vaporization rate is the most sensitive variable observed on  $\text{LaB}_6$  emitters, depending strongly on unpredictable stoichiometric variations. Comparison by Swanson et al.<sup>19</sup> with work function data indicates a certain correlation, however, less than would be expected on the basis of the large observed changes of the activation energies. This leads to the conclusion that the surface of the crystal reaches equilibrium near stoichiometry much more rapidly than the bulk. The vaporization appears diffusion limited from the bulk.

In experiments<sup>18</sup> leading to emission plots shown in Fig. 14, it was observed that the emission from (110) crystal surfaces at  $1400^\circ\text{C}$  at  $5 \times 10^{-6}$  Torr pressure (by a crystal of low impurity content) exhibited a gradual change of work function from 2.86 eV to 3.1 eV within 50 hours. In oxygen of the same pressure the change occurred more rapidly. The changes were accompanied by the formation of a hill and valley structure on the surface. Through LEED analysis it was determined that faceting occurred where small areas of  $1 \mu\text{m}^2$  or less recrystallized into the much more stable (111) configuration. The (111) surface, however, has a higher work function (3.4 eV) and, therefore, the emission decreases. Adsorption of monolayers of oxygen with subsequent evaporation at  $1400^\circ\text{C}$  at  $10^{-10}$  Torr only very gradually removed the (111) spots. No such faceting was observed on the other crystal surfaces.

Clearly this phenomenon is crucial for emission stability and requires further attention when considering  $\text{LaB}_6$  for long lifetime cathodes.

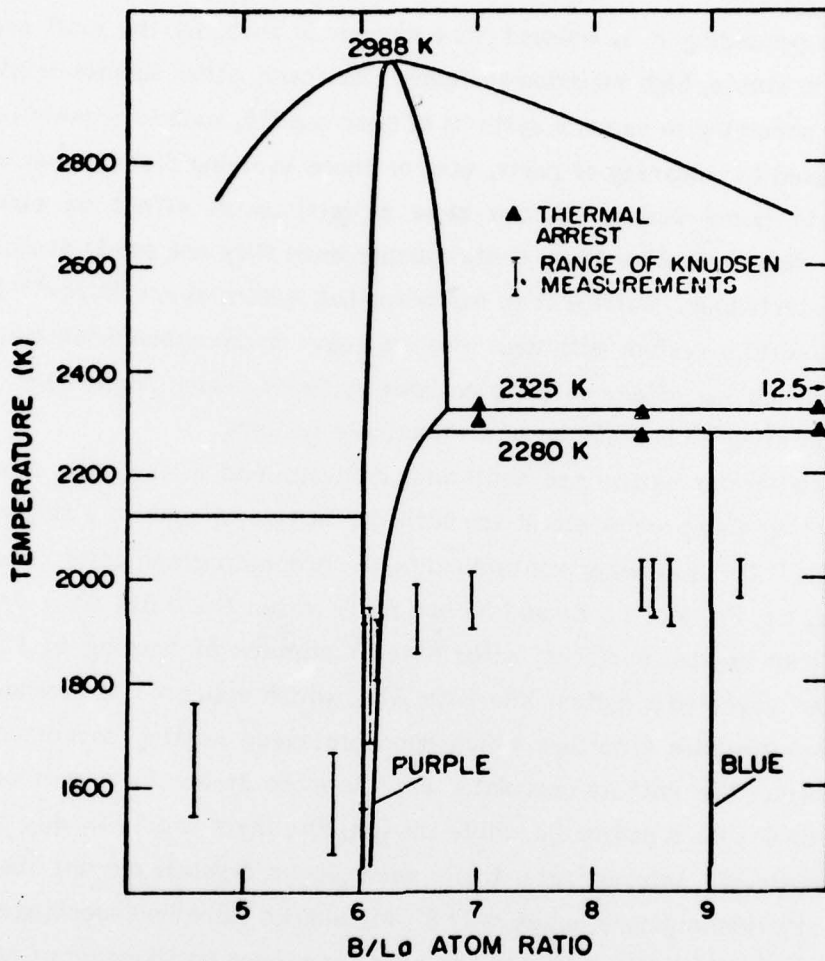


Fig. 17. Partial phase diagram of the La-B system in the region of  $\text{LaB}_6$ . The composition and temperature range of Knudsen studies are indicated.<sup>22</sup>

### Surface Contamination

From the preceding it is evident that oxygen is probably the most serious "contaminant" to stable, high emission surfaces. However, other surface contaminants typically occurring in vacuum systems of poor quality, such as organic vapors from solvents used for cleaning of parts, etc. or those evolving from rubber seals, or those due to pump fluids, all can have a detrimental effect on emission properties. We do not consider these contaminants since they are easily avoided by proper vacuum technique. Suffice it to say here that Avdienko and Malev<sup>23</sup> found that CO admitted to a system with high level of heavy hydrocarbon contamination can have a rejuvenating effect on dirty cathode surfaces, which might be of some utility when operating e-beams in large demountable systems.

Of a more serious nature are contaminants contained in the  $\text{LaB}_6$  material which upon heating may precipitate at the surface. In typical runs on a singly zone refined crystal<sup>24</sup> the following contaminants were spectrographically detected: Co, Si, Mn, Hg, Cr, Fe, Mo, Ti, Zr and Ni but no C within the 0.044 wt% limit of detection. Clean crystal surfaces, after several minutes of heating to 1300 to 1600C, however, revealed a carbon line with AES, which appeared to arrange in a two dimensional graphite structure which upon prolonged heating converted to a more stable form. The authors postulate that the more stable form represents a bonding state of C with B and/or La, while the graphite layer is only weakly bonded to the  $\text{LaB}_6$  substrate. Interestingly, triple zone passed crystals did not show any carbon contamination anymore, while only Si, Mg and Fe remained spectrographically detectable. These results indicate the need for proper purification of cathode materials.

### Fabrication of Metallic Hexaboride Crystals

The aforementioned properties indicate that metallic hexaborides require special techniques in the growth of their single crystals. Of particular importance is the high melting point. As seen in Fig. 17, the melting point of  $\text{LaB}_6$  can be as high as 2700°C while that for  $\text{CaB}_6$  is approximately 2235°C. Production of a pure

melt of these materials would require high temperature technology which may not be economic or desirable for other reasons. Fortunately, there are other options available. They are:

- (a) crystallization using a molten flux
- (b) vapor phase crystallization
- (c) electrolytic crystallization
- (d) zone refinement of hot pressed powders.
- (e) growth from melt

In the following these processes are described with particular reference to the growth of  $\text{LaB}_6$  single crystals.

(a) Crystallization Using a Molten Flux

Although the details of experimental methods may vary, the basic process is the same and depends on the use of a non-reactive molten flux as a medium allowing the free motion of the solute atoms in the solvent. In the growth of  $\text{LaB}_6$ , the flux is typically aluminum which has a melting point of  $660^\circ\text{C}$  and is easily dissolved away when the processing is done. The melt is composed of Al powder (325 mesh) 97 wt% and 3 wt%  $\text{LaB}_6$  powder (325 mesh). In place of the  $\text{LaB}_6$  compound, powders of pure La and B have been used<sup>25</sup> (2 wt% La to 12 wt% B). The mixture is placed in an alumina crucible and heated rapidly in an argon atmosphere to a temperature  $\approx 1200^\circ\text{C}$ . (The argon atmosphere is necessary because metal hexaborides are susceptible to surface oxidation.) It is held at this temperature for some period of time and then slowly cooled to room temperature.

As previously stated, the details of this process vary. Aita et al.<sup>25</sup> heated the mixture to  $1500^\circ\text{C}$  and held it at this temperature for 8 hours, while Futamoto et al.<sup>26</sup> heated the mixture to  $1200^\circ\text{C}$  and held it for 5 to 10 hours. Present work indicates holding at  $1400^\circ\text{C}$  for 6 hours is sufficient to allow for a complete mixing of solute atoms throughout the solvent. Although the actual atomic processes are not known at this time, it is postulated that the elevated temperature allows each species to dissociate into individual atoms in the solution; when cooling begins, the atoms migrate into energetically favorable bonding orientations. Factors such as ionic size, electronegativity and symmetry of the bond structure influence the final

structure.

The rate of cooling also varies; Futamoto et al.<sup>26</sup> varied the cooling rate from 6 to 75°C/hour. They found that the thickness of the resulting crystals of needle-like appearance decreased with an increased cooling rate. The rate must be slow enough to allow effective diffusion of La and B through the solvent as well as allowing for the reaction to occur at the interface of the crystal.

After the solution has cooled to room temperature, the solid aluminum is removed with HCl or NaOH solutions. The crystals form three shapes: cubes, platelets and needles. The cubic crystals average 1 mm<sup>3</sup> whereas the needles are about 5 mm long and have a cross section of 0.1 to 0.5 mm<sup>2</sup>.

The habit plane for the growth of the crystals is the (100) face, and these faces form the sides of the cubes and plates. The growth direction is  $\langle 100 \rangle$ .

#### (b) Vapor Phase Crystallization

Vapor phase crystallization is accomplished by the use of a quartz tube apparatus with two sight holes for measuring the temperature as done by Niemyski et al.<sup>27</sup> A graphite chamber is placed inside the quartz tube; this is heated inductively, providing two different temperature zones. The first zone is pressurized with boron trichloride (BCl<sub>3</sub>) and hydrogen, and is heated to 1000°C. A tablet of pressed LaB<sub>6</sub> is placed in this chamber where it reacts with the gases. This vapor is then transported to the second zone where the temperature is raised to 1350-1450°C. Here, the crystals are formed. Experimental results show that the size and habit plane are influenced by the temperatures and the gas flow rate as well as the proportions of BCl<sub>3</sub> and H<sub>2</sub> used.

This process produced crystals which were cubic, ranging up to 1 mm<sup>3</sup>. These crystals are in the form of octahedra with (111) habit planes, or cubes with (100) habit planes. Niemyski et al.<sup>27</sup> state that by lowering the temperature in the second zone to 1300°C, layers of LaB<sub>6</sub> could be deposited on a substrate, forming emission coatings on a surface.

#### (c) Electrolytic Crystallization

One of the major advantages of electrolytic crystallization is that growth processes may be studied in detail due to the fact that the growth rate can be

varied directly by an adjustment of the current flow. The linear growth rate of the crystals,  $\nu$ , is related to the current density,  $i$ , by

$$\nu = \frac{i \epsilon \Omega}{2 F}$$

where  $\Omega$  is the molar volume ( $77.8 \text{ cm}^3 \text{ mole}^{-1}$  for  $\text{LaB}_6$  at RT),  $F$  is Faraday's constant, 2 is the number of electrons to deposit one molecule, and  $\epsilon$  is the current efficiency factor. The maximum stable growth rate, according to Elwell, et al.<sup>28</sup>, is approximately  $1 \times 10^{-6} \text{ cm sec}^{-1}$  which corresponds to an applied current density of  $30 \text{ mA cm}^{-2}$  for  $\epsilon = 1$ .

The components of the electrolytic melt (2.2 mol%  $\text{La}_2\text{O}_3$ , 33.5 mol%  $\text{B}_2\text{O}_3$ , 31.2 mol%  $\text{Li}_2\text{O}$  and 33.1 mol%  $\text{LiF}$ ) were placed in a nickel crucible under a helium atmosphere. The growth occurred at  $800^\circ\text{C}$  on a gold wire cathode 0.075 mm in diameter. The anode was gold foil about  $1 \text{ cm}^2$ . The cell potential was maintained between 1.85 and 2.0 V. This process produced crystals in a mass with cubic (100) habit planes.

The crystals grew in terraces with a (100) face which grew slowly across the crystal face. As the current density is lowered, these pyramidal projections are reduced in relation to the overall dimensions of the crystal. If the current is raised, dendritic projections begin to occur from the corners of the cubes. These dendrites are projected in the  $\langle 100 \rangle$  directions, and the sides of the dendrites were formed from (100) terraces.

#### (d) Zone Refinement

One procedure to be discussed is the primary method of producing  $\text{LaB}_6$  cathodes for use in electron microscopy.<sup>29</sup> The  $\text{LaB}_6$  powder is hot-pressed into tablets. An arc float zone technique is used which zone refines and partially crystallizes the hot pressed tablet. As a current is passed through the material, a small molten zone is formed in the tablet. As this zone moves through the material, impurities are forced to move into the molten zone as the  $\text{LaB}_6$  recrystallizes. These impurities move to the end of the crystallized material and

are trapped there where they can be cropped off. Five or six passes of this nature will produce a  $\text{LaB}_6$  cathode with an impurity content of  $\approx 1$  ppm. However, this material is still a polycrystalline material.

A slight modification of this procedure produces high purity  $\text{LaB}_6$  crystals by multi-float zone passage.<sup>30</sup> Polycrystalline rods are heated by RF induction heating under pressurized argon gas ( $15 \text{ kg/cm}^2$ ). The extent of purity attained after three zone passages can be judged from the fact that a resistivity ratio as high as 450 was measured between room and liquid helium temperature. Again the final product is not exactly single crystalline but consists of subgrains with sizes of order  $1 \text{ mm}^3$ . Maximum misorientation is reported to be a few degrees. Crystal dimensions as large as 7 mm diameter by 60 mm length have been obtained.

(e) Growth from Melt

The most significant problem to be faced in the growth of single crystal metal hexaborides is that of creating an environment with a high enough temperature to exceed the melting point of these materials. If temperatures of  $\approx 2700^\circ\text{C}$  can be achieved, and the resultant melt can be properly contained and controlled, it will be possible to produce much larger single crystals through a pulling of Czochralski technique using a seed crystal which is rotated as it is withdrawn from the melt. No crystal growth by this procedure has been reported as yet.

### CONCLUSION

Obviously, a lot remains to be done to complete our understanding of the physical properties of  $\text{LaB}_6$  and other metal hexaborides. More experimental results on band structure information at the various crystal surfaces is required in order to provide a basis against which to check and, if necessary, to improve theory. For elucidation of electron transport processes, phonon spectra are needed, where very little information is presently available. Electron-phonon interactions and resultant superconducting properties of hexaborides in general remain of great interest and presently afford considerable attention within the scientific community.

The emission properties of  $\text{LaB}_6$  and other  $\text{MB}_6$  compounds also need further clarification. Evaporation rates of constituents, crystal surface structure and stability in the presence of oxygen and other tube gases as well as most desirable metal constituents for large emission currents remain to be firmly established. The manufacture of large, truly single crystals (5 mm dia) will not only help experimentation on other than (100) surfaces but also establish the use of the  $\text{LaB}_6$  compound as cathode material for large current density e-beam generation in power devices.

### References

1. "Role of polar optical phonon scattering in electrical resistivities of  $\text{LaB}_6$  and  $\text{Re O}_3$ ", T. Tanaka, T. Akahane, E. Bamai, S. Kawai, N. Tsuda and Y. Ishizawa, *J. Phys. C. Solid St. Phys.* **9**, 1235 (1976).
2. "Energy bandstructure and Fermi surface of  $\text{LaB}_6$  by a self consistent APW method," A. Hasegawa and A. Yanase, *J. Phys. F., Metal Phys.* **7**, 1245 (1977).
3. "The electronic structure of the borides  $\text{MB}_6$ ", H.C. Longuet-Higgins and M. de V. Roberts, *Proc. Roy. Soc.* **224**, 336 (1954).
4. "The valence band structure of metal hexaborides: an ESCA study of  $\text{CaB}_6$  and  $\text{Y B}_6$ ," M. Aono, S. Kawai, S. Kono, M. Okusawa, T. Sagawa and Y. Takehana, *J. Phys. Chem. Solids* **37**, 215 (1976).
5. "Surface states of  $\text{LaB}_6$  (001) as revealed by angular-resolved ultraviolet photoelectron spectroscopy," M. Aono, T. Tanaka, E. Bannai, C. Oshima and S. Kawai, *Phys. Rev. B* **16**, 3489 (1977).
6. "Optical properties of rare earth hexaborides," T. Suzuki, Y. Isikawa, T. Tanaka, K. Takegahara and T. Kasuya, US-Japan Seminar, Sendai, Oct. 1977, p. 205.
7. "Plasma reflection edge in crystalline  $\text{MB}_6$  compounds," E. Kierzek-Pecold, *Phys. Stat. Sol.* **33**, 523 (1969).
8. "de Haas-van Alphen effect and the Fermi surface of  $\text{LaB}_6$ ," A. J. Arko, G. Crabtree, D. Karim, F. M. Mueller, L.R. Windmiller, J. B. Ketterson and Z. Fisk, *Phys. Rev. B* **13**, 5240 (1976).
9. "de Haas-van Alphen effect and Fermi surface of  $\text{LaB}_6$ ," Y. Ishizawa, T. Tanaka, E. Bannai and S. Kawai, *J. Phys. Soc. Japan* **42**, 112 (1977).
10. "Raman spectra of metallic and semiconducting metal hexaborides ( $\text{MB}_6$ )," M. Ishii, M. Aono, S. Muranaka and S. Kawai, *Sol.Stat. Comm.* **20**, 437 (1976).
11. "Raman scattering in metallic  $\text{LaB}_6$ ," M. Ishii, T. Tanaka, E. Bannai and S. Kawai, *J. Phys. Soc. Japan* **41**, 1075 (1976).
12. "Preparation of lanthanum hexaboride by electrolysis and measurements of the raman active phonons," H. Scholz, W. Bauhofer and K. Ploog, *Solid Stat. Comm.* **18**, 1539 (1976).
13. "Large electron-phonon interaction but low temperature superconductivity in  $\text{LaB}_6$ ," A. J. Arko, et al., *International Journal of Quantum Chemistry Symp.* No. 9, 569 (1975).

14. "Characterization of clean and oxidized (100)  $\text{LaB}_6$ ," B. Goldstein and D. J. Szostak, (to be published).
15. "Structure of the  $\text{LaB}_6$  (001) surface studied by angle resolved XPS and LEED," M. Aono, C. Oshima, T. Tanake, E. Bannai and S. Kawai, *J. Appl. Phys.* **49**, 2761 (1978).
16. "Anisotropy of thermionic electron emission values for  $\text{LaB}_6$  single crystal emitter cathodes," P. H. Schmidt, D. C. Joy, L. D. Longinotti, H. J. Leamy, S. D. Ferris and Z. Fisk. *Appl. Phys. Lett.* **29**, 400 (1976).
17. "Field emission and field ion microscopy of lanthanum hexaboride," M. Futamoto, S. Hosoki, H. Okano and U. Kawabe, *J. Appl. Phys.* **48**, 3541 (1977).
18. "Thermionic work function of  $\text{LaB}_6$  single crystals and their surfaces," C. Oshima, E. Bannai, T. Tanaka and S. Kawai, *J. Appl. Phys.* **48**, 3925 (1977).
19. "Fabrication and surface characterization of composite refractory compounds suitable for thermionic converter," L. W. Swanson, M. Gesley and D. R. McNeely, NASA LRC, Cleveland Interim Rept. No. 2, Grant No. NSG-3054
20. "Auger electron spectroscopy study of oxidation on  $\text{LaB}_6$ ," C. Oshima and S. Kawai, *Appl. Phys. Lett.* **23**, 215 (1973).
21. "Single-crystal workfunction and evaporation measurements of  $\text{LaB}_6$ ," L. W. Swanson and T. Dickinson, *Appl. Phys. Lett.* **28**, 578 (1976).
22. "Phase relationship, vaporization, and thermodynamic properties of the lanthanum-boron system," E. Storms and B. Mueller, *The Journal of Physical Chemistry*, **82**, 51 (1978).
23. "Poisoning of  $\text{LaB}_6$  cathodes," A. A. Avdienko and M. D. Malev. *Vacuum* **27**, 583 (1977).
24. "Carbon layer on lanthanum hexaboride (100) surface," C. Oshima, E. Bannai, T. Tanake and S. Kawai, *Jap. Appl. Phys.* **16**, 965 (1977).
25. "Single crystal growth of lanthanum hexaboride in molten aluminum," T. Aita, V. Kawake and Y. Honda, *Japan J. Appl. Phys.* **13**, 391 (1974).
26. "Crystallographic properties of  $\text{LaB}_6$  formed in molten aluminum," M. Futamoto, T. Aita and U. Kawabe, *Jap. J. Appl. Phys.* **14**, 391 (1975).

27. "Crystallization of lanthanum hexaboride," T. Niemyski and E. Kierzek-Pecold, *J. of Crystal Growth*, 3, 162 (1968).
28. "Surface structure and electrolytic growth stability of  $\text{LaB}_6$  crystals," D. Elwell, I. V. Zubeck, R. S. Feigelson and R. A. Huggins, *J. of Crystal Growth*, 29, 65 (1975).
29. "Influence of crystallography and purity on brightness of  $\text{LaB}_6$  cathodes," J. D. Vehoeven, E. D. Gibson, and M. A. Noack, *J. Appl. Phys.* 47, 5105 (1976).
30. "Growth of high purity  $\text{LaB}_6$  single crystals by multi-float zone passage," T. Tanaka, E. Bannai, S. Kawai and T. Yamane, *J. Crystal Growth* 30, 193 (1975).

## LABORATORY OPERATIONS

The Laboratory Operations of The Aerospace Corporation is conducting experimental and theoretical investigations necessary for the evaluation and application of scientific advances to new military concepts and systems. Versatility and flexibility have been developed to a high degree by the laboratory personnel in dealing with the many problems encountered in the nation's rapidly developing space and missile systems. Expertise in the latest scientific developments is vital to the accomplishment of tasks related to these problems. The laboratories that contribute to this research are:

**Aerophysics Laboratory:** Launch and reentry aerodynamics, heat transfer, reentry physics, chemical kinetics, structural mechanics, flight dynamics, atmospheric pollution, and high-power gas lasers.

**Chemistry and Physics Laboratory:** Atmospheric reactions and atmospheric optics, chemical reactions in polluted atmospheres, chemical reactions of excited species in rocket plumes, chemical thermodynamics, plasma and laser-induced reactions, laser chemistry, propulsion chemistry, space vacuum and radiation effects on materials, lubrication and surface phenomena, photo-sensitive materials and sensors, high precision laser ranging, and the application of physics and chemistry to problems of law enforcement and biomedicine.

**Electronics Research Laboratory:** Electromagnetic theory, devices, and propagation phenomena, including plasma electromagnetics; quantum electronics, lasers, and electro-optics; communication sciences, applied electronics, semi-conducting, superconducting, and crystal device physics, optical and acoustical imaging; atmospheric pollution; millimeter wave and far-infrared technology.

**Materials Sciences Laboratory:** Development of new materials; metal matrix composites and new forms of carbon; test and evaluation of graphite and ceramics in reentry; spacecraft materials and electronic components in nuclear weapons environment; application of fracture mechanics to stress corrosion and fatigue-induced fractures in structural metals.

**Space Sciences Laboratory:** Atmospheric and ionospheric physics, radiation from the atmosphere, density and composition of the atmosphere, aurorae and airglow; magnetospheric physics, cosmic rays, generation and propagation of plasma waves in the magnetosphere; solar physics, studies of solar magnetic fields; space astronomy, x-ray astronomy; the effects of nuclear explosions, magnetic storms, and solar activity on the earth's atmosphere, ionosphere, and magnetosphere; the effects of optical, electromagnetic, and particulate radiations in space on space systems.

THE AEROSPACE CORPORATION  
El Segundo, California

...